Fatigue properties of a pseudoelastic NiTi alloy: Strain ratcheting and hysteresis under cyclic tensile loading

C. Maletta [a], E. Sgambitterra [a,*], F. Furgiuele [a], R. Casati [b], A. Tuissi [c]

[a] Department of Mechanical, Energy and Management Engineering, University of Calabria, Ponte P. Bucci 46 C, 87036 Rende, CS, Italy
[b] Department of Mechanical Engineering, Politecnico di Milano, Via La Masa 34, 20100 Milano, Italy
[c] National Research Council—Institute for Energetics and Interphases, Corso Promessi Sposi 29, 23900 Lecco, Italy

Article history:
Received 10 December 2013
Received in revised form 11 March 2014
Accepted 17 March 2014
Available online 27 March 2014

1. Introduction

NiTi shape memory alloy has become, in the last years, increasingly important in different applications field, as a consequence of their peculiar properties [1], shape memory, pseudoelasticity, corrosion resistance-that make it favorable to realize biomedical implants, dentistry, aerospace, engineering and sports equipment. However, due to the solid phase transformation mechanisms, involving this special alloy, unusual fracture and fatigue response has to be expected, therefore standard testing procedures to identify its fatigue and fracture response cannot be applied. Fatigue loads cause a big modification of the global response of NiTi alloys, due not only to the mechanical damage imposed by the cyclic load, but, especially, to the functional evolution related to the phase transition mechanisms.

As a consequence of these peculiar properties, both structural and functional fatigue behavior of NiTi alloys is still unknown. To this aim, starting from Melton's pioneering work [2], some experimental studies were carried out in the last few years to analyze the fatigue behavior of NiTi alloys, by using non-standard specimens and testing procedures [3,4]. In particular, in most of these works the cyclic behavior of NiTi wires [5–16], subjected to rotating bending conditions were analyzed, and in one of them [12] an unusual behavior ("*z-shape*" response), in terms of applied strain-number of cycles to failure, is reported. Furthermore, NiTi tubes [17–23] were analyzed, in terms of both crack propagation rate and fatigue life estimation. In fact, stress induced phase transition mechanisms occurs in the crack tip region [24–27], which significantly affects the stress distribution and, consequently, the local values of the stress intensity factor [28,29]. Moreover, in order to better investigate the fatigue properties of such components, diamond-shaped samples were studied [30], with geometry very close to the unit cell of a stent. Furthermore, other studies [31,32] were carried out on single crystal specimens, cut along different crystallographic orientations, in order to investigate the functional behavior of NiTi alloys. In particular, fatigue resistance and functional evolution, for different orientations, were investigated in [31], while the influence of different heat treatments and of precipitates, were studied in [32]. In addition, the evolution of damping properties and the seismic damping capabilities of pseudoelastic SMAs was analyzed in [33,34], while the modification of the shape memory properties of thin wire for actuators was analyzed in [35,36].

Within this context, a low cycle fatigue study of a pseudoelastic NiTi sheet in the stress-induced transformation regime was undertaken. Each test was carried out in two subsequent steps: (i) material stabilization and (ii) fatigue life estimation. In the first step, to avoid compression stresses during unloading, a variable strain

* Corresponding author. Tel.: +39 0984494698.
E-mail address: esgambitterra@unical.it (E. Sgambitterra).

ratio was adopted until the mechanical stabilization of the alloy. Subsequently, the stabilized specimens were subjected to strain controlled fatigue tests, under a fixed strain ratio, up to complete failure. In this paper, based on experimental tests carried out in a previous study [37], where investigations on the structural fatigue properties of the alloy were carried out (second step), the strees–strain response was accurately monitored in the first step, in order to analyze the evolution of the functional properties of the alloy in terms of pseudoelastic recovery capabilities. In particular, this evolution was systematically analyzed by identifying several functional damage parameters, involving strain, energy, transformation stress, Young's modulus and phase transition temperatures.

Results on functional fatigue, in terms of pseudoelastic evolution response, and on structural fatigue, in terms of cycles to failure, are here reported and discussed.

2. Materials and experimental methods

A commercial pseudoelastic Ni-rich NiTi sheet (50.8 at.% Ni–49.2 at.% Ti, Memry, Germany) with thickness $t = 1.5$ mm, was analyzed. Dog bone shaped specimens, with gauge length of 10 mm, were cut from *as received* sheets by wire electro discharge machining. A polishing of the machined surfaces was subsequently carried out by sandpapers with progressively finer grits (#400–#1200) and finally by diamond paste (5 μm).

Fig. 1a illustrates stress–strain curve of the *as received* material obtained from an isothermal ($T = 298$ K) loading–unloading cycle, with a strain rate $\dot{\varepsilon} = 2.510^{-2}$ s^{-1}, up to complete stress-induced martensitic transformation corresponding to a maximum strain of about 6.2%. Deformations were measured by means of an extensometer with a gauge length of 10 mm. The figure also shows the values of the main thermo-mechanical parameters of the alloy, in terms of Young's moduli (E_A,E_M), transformation stresses $\left(\sigma_s^{AM}, \sigma_f^{AM}, \sigma_s^{MA}, \sigma_f^{MA}\right)$, and transformation strain (ε_L). Fig. 1b illustrates a Differential Scanning Calorimetry (DSC) curve of the *as received* material which was performed over a temperature range between −100 °C and 100 °C using a heating/cooling rate of 10 °C/min (DSC Seiko 220C). The graph clearly shows a two-stage direct transformation from high temperature parent phase (*B2*) to rhombohedral phase (*R*) to low temperature stable phase (*B19′*). In contrast, a one-stage inverse transformation *B19′–B2* characterizes the heating branch of the curve. This is a typical curve of NiTi after aging, indeed the formation of Ti_3Ni_4 precipitates are responsible of the change of the transformation path from *B2–B19′* to *B2–R–B19′* [1].

Fatigue tests were carried out, under isothermal condition ($T = 298$ K) by using a universal servo-hydraulic testing machine (Instron 8500) equipped with a climatic chamber (MTS 651).

Due to the cyclic creep-like behavior of NiTi alloys, which causes the accumulation of residual deformations in the first mechanical cycles ($\delta\varepsilon_{resi}$), as illustrated in Fig. 2, fatigue tests were carried out in two subsequent steps, as described in [37]: (1) Material stabilization and (2) Fatigue life estimation. In particular, in the first step a variable strain ratio was adopted, in order to avoid compression stresses during unloading, and the strain ratcheting mechanisms were analyzed up to a stable mechanical response of the alloy, corresponding to N_s cycles. The transition evolution was monitored during the first few N_s cycles in order to investigate on the loss functional capability of the alloy. The number of cycles to stabilization, N_s, was defined based on the evolution of residual deformations, in particular when the increment of ε_{res} in the previous 10 cycles is lower than 0.005 ε_{max} $\left(\sum_{i=N_s-10}^{N_s}\delta\varepsilon_{res\ i} < 0.005 \cdot \varepsilon_{max}\right)$.

In the second step, the specimens were subjected to strain controlled fatigue cycles at a frequency of 0.5 Hz, under a fixed strain ratio and with a strain range $\varepsilon = 2\varepsilon_a$, were carried out up to complete failure and the corresponding number of cycles N_f has been recorded.

Several tests were carried out for different values of the maximum strain, ε_{max}, within the pseudoelastic regime of the alloy, *i.e.* in the range between 0.7% and 4.5% and at least two specimen for each testing conditions were analyzed.

3. Results and discussions

In the following sections the evolution on the functional properties of the alloy mainly occurring in the first step of fatigue tests are illustrated. In addition, structural fatigue data, in terms of number of cycles to failure versus applied strain, are reported and analyzed by a modified Coffin–Manson approach [37], together SEM analysis of the fracture surfaces.

3.1. Functional fatigue

The modification of the hysteretic stress–strain response of the material obtained under repeated isothermal mechanical cycles involving stress induced transformations can be attributed to several microstructural mechanisms, such as the formation of stabilized martensite, detwinning, grain reorientation, slips deformations and the generation of lattice defects mainly in the form of

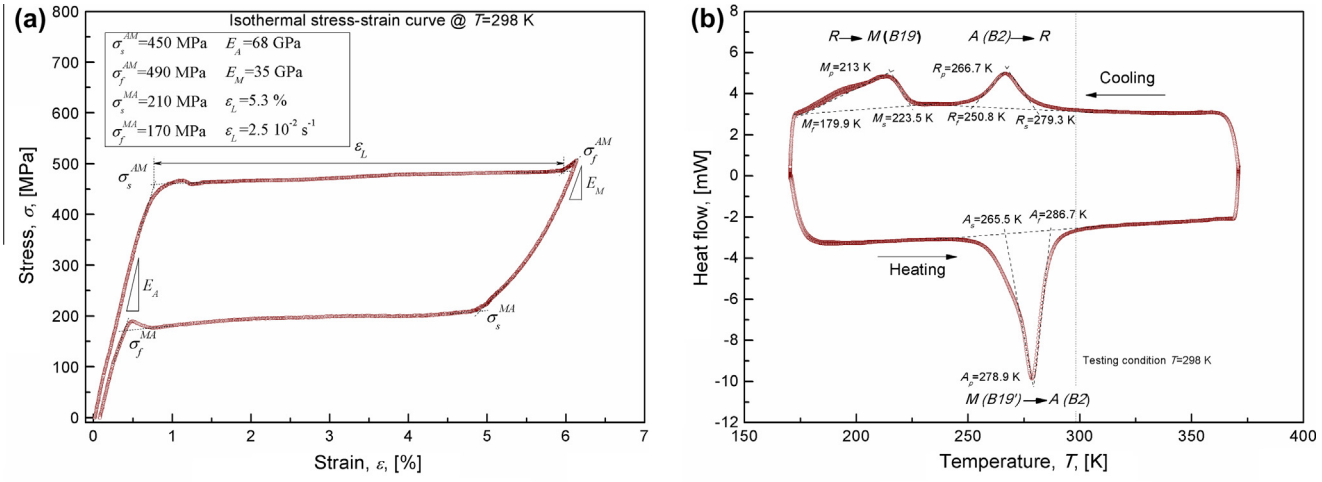

Fig. 1. Thermo-mechanical properties of the *as received* material: (a) isothermal ($T = 298$ K) stress strain curve and (b) DSC plot.

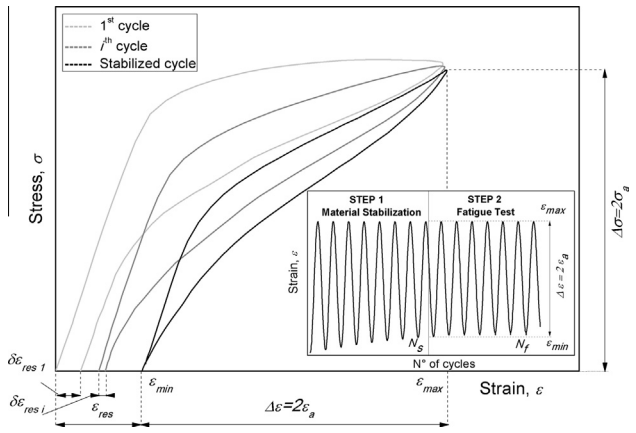

Fig. 2. Schematic depiction of the evolution of the stress–strain hysteretic loops under cyclic loadings at fixed values of maximum strain [37].

dislocations [38,39]. In particular, upon repeated loadings, many preferentially oriented martensite variants reach stress conditions that inhibit the possibility to recover their original configuration, and the dislocation density tends to increase, as a consequence of shear deformations at the martensite-austenite interfaces. These microstructural evolutions cause a gradual loss of functional properties, *i.e.* the capability to dissipate energy and to recover the applied deformation, with a consequent increase of residual strain and decrease of the hysteresis loop area, as schematically illustrated in Fig. 2. In this work the functional fatigue properties are deeply analyzed by identifying and tracking the evolution of several functional fatigue parameters, as schematically shown in Fig. 3:

(1) recovered strain, ε_{rec}: pseudo-elastic recovery from mechanical unloading;
(2) residual strain, ε_{res}: unrecovered strain upon unloading;
(3) recovered energy, E_{rec}: energy below the unloading branch of the hysteresis loop;
(4) dissipated energy, E_{diss}: energy between loading and unloading paths of the hysteresis loop;
(5) effective Young's modulus, E_A: slope of the first elastic response in the σ−ε diagram;
(6) direct transformation stress, σ_s^{AM}: intersection between elastic straight line and tangent to the stress plateau [5];

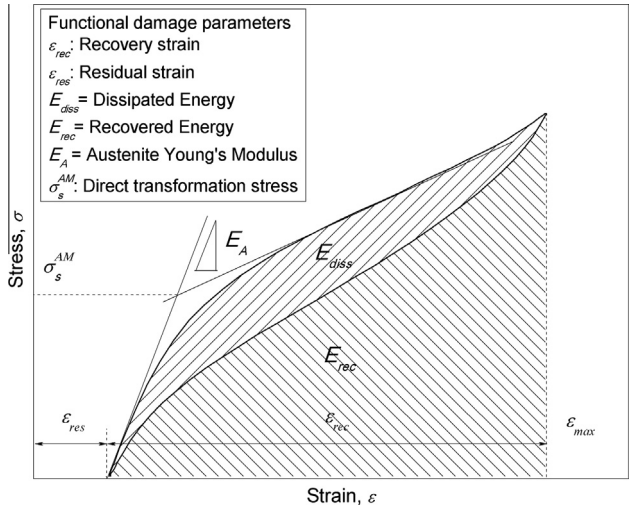

Fig. 3. Schematic depiction of the functional damage parameters.

In addition, phase transition temperatures of the specimens, after fatigue tests, were investigated by DSC measurements.

In the following subsections the results concerning the evolution of the aforementioned functional fatigue parameters are reported and discussed, while in Table 1 some summary data are illustrated. In particular, this table reports the values of the parameters after material stabilization (cycle N_s) together with the reference values at the first mechanical cycle (cycle #1). It is worth noting that reported data are the average values (μ) of different specimens subjected to the same testing conditions and, as indicated by the maximum coefficient of variation ($c_v = \sigma/\mu$), defined as the ratio between the standard deviation (σ) and the average value of each parameter, no significant variation of the functional response has been observed among them.

3.1.1. Recovered and residual strain

Recovery and residual strains, ε_{rec} and ε_{res}, are important functional fatigue parameters because they represent a quantitative measure of the cyclic evolution of the pseudoelastic properties of the alloy during loading history. Fig. 4 reports the evolution of ε_{rec} (Fig. 4a) and ε_{res} (Fig. 4b) as a function of the number of mechanical cycles and for different values of the maximum strain, ε_{max}, in pseudo-elastic regime of the alloy, *i.e.* in the range between 0.7% and 4.5%. As expected, a rapid increase of ε_{res}, with an associated decrease of ε_{rec}, occurs during the first few cycles, mainly because of the plastic deformation related to the martensitic transformation and the mechanical loading. Moreover, lattice defects may lead to martensite stabilization [40–43]. Nevertheless, the material reaches a pseudoelastic steady state condition with increasing the number of cycles. These phenomena are more evident for the higher values of applied deformation by which an higher evolution rate has been registered; on the contrary the number of cycles to stabilization N_s, which is always between 100 and 140, seems to be unaffected by the strain amplitude. Similar results have been obtained in previous researches [20,23] even in the case of single crystal alloys [32]. It is a unusual behavior if compared with common metals, where the stabilization of the stress–strain response of the material, due to repeated plastic deformations, is related to the cycles to failure and, consequently, to the strain amplitude [44]. In addition, Fig. 4a and Table 1 also show that pseudoelastic strain recovery capabilities of the SMA are mainly preserved, with stabilized values of ε_{rec} ranging from 72% to 97% of ε_{max}, at ε_{max} = 4.5% and 0.7% respectively.

Fig. 5 reports the stabilized values of ε_{res} and ε_{rec} as a function of the maximum applied strain, ε_{max}, in a log–log diagram and a linear trend of both parameters is observed. In particular, ε_{res} ranges from about 0.01% at ε_{max} = 0.70–1.30% at ε_{max} = 4.50% and, as a consequence, ε_{rec} ranges from about 0.69% to about 3.20%. Complete are reported in Table 1.

3.1.2. Recovered and dissipated energy

As described in the previous sections and schematically depicted in Fig. 3, repeated mechanical cycles cause a modification of the whole stress–strain hysteretic behavior of the alloy, *i.e.* they affect not only the pseudoelastic strain recovery capability but also the shape of the stress–strain hysteretic loop. As a consequence, a marked modification of the recovered and dissipated energy, E_{rec} and E_{diss} (see Fig. 3), has been observed and the knowledge of this trend is of major concern, especially when dealing with the design of energy absorber devices, such as seismic absorbers [33]. Fig. 6 reports the evolution E_{rec} (Fig. 6a) and E_{diss} (Fig. 6b) as a function of the number of mechanical cycles and for different values of the maximum strain, ε_{max}.

As expected, a rapid decrease of both parameters occurs during the first few cycles, as a direct consequence of the development of

Table 1
Values of the functional fatigue parameters obtained from material stabilization.

ε_{max}	ε_{res}, (%)		ε_{rec}, (%)		E_{diss}, (MJ/m^3)		E_{rec}, (MJ/m^3)		E, (GPa) (Cycle #1 E_A = 68 GPa)	σ_s^{AM}, (MPa) (Cycle #1 σ_s^{AM} = 450 MPa)
	Cycle #1	Cycle N_s	Cycle #1	Cycle N_s	Cycle #1	Cycle N_s	Cycle #1	Cycle N_s		
0.70%	0.01	0.02	0.69	0.68	0.45	0.03	2.11	1.23	67.3	
1.00%	0.01	0.04	0.99	0.96	0.80	0.09	2.97	1.99	66.4	355
1.30%	0.01	0.06	1.29	1.24	1.15	0.23	3.87	2.65	65.0	342
1.45%	0.01	0.09	1.44	1.36	1.40	0.42	4.78	3.26	63.5	331
1.70%	0.02	0.14	1.68	1.56	1.72	0.60	5.23	3.84	62.2	322
2.00%	0.03	0.16	1.97	1.84	2.10	0.81	5.84	4.25	61.9	301
2.40%	0.06	0.29	2.33	2.11	2.66	1.02	7.40	5.32	60.7	285
3.00%	0.07	0.59	2.92	2.41	3.29	1.21	8.50	5.59	58.1	250
3.50%	0.08	0.84	3.42	2.66	4.89	1.42	9.71	6.14	54.2	239
4.00%	0.16	0.95	3.83	3.05	5.87	1.81	10.82	6.88	49.4	227
4.50%	0.20	1.24	4.30	3.26	7.37	2.38	12.45	7.64	44.9	215
c_v	0.04	0.03	0.01	0.01	0.04	0.06	0.02	0.04	0.03	0.02

residual deformations (see Fig. 4b), and this effect becomes more evident as ε_{max} increases. However, a higher reduction rate of the dissipated energy has been observed, which can be attributed to plastic deformation and to an increase of dislocation density. Dislocations may lead to the formation of stress field into the lattice and then to the formation of stabilized martensite induced by stress [40–43]. In fact, E_{diss} is strictly related to the hysteresis in the stress-induced phase transition mechanisms. In particular, Fig. 6b and Table 1 show that stabilized values of E_{diss} are between 30% and 40% of the values of the first cycles for ε_{max} > 1.30%, while even more marked reductions are observed for the lower values of ε_{max}, because these latter are very close to the elastic limit of the material (σ_s^{AM}) and, consequently, the hysteretic behavior tends to vanish. This trend should be accurately taken into account in the design of energy absorber and seismic devices operating under low cycle regime, as it implies a marked degradation of their functional response. Alternatively, proper training processes of the material should be carried out in order to obtain a stable functional response.

Fig. 7 reports the stabilized values of E_{rec} and E_{diss} as a function of the maximum applied strain, ε_{max}, in a semi-log diagram. The figure show that E_{rec} ranges from about 1.22 MJ/m^3 at ε_{max} = 0.70% to 7.64 MJ/m^3 at ε_{max} = 4.50%, while E_{diss} ranges from about 0.03 MJ/m^3 to about 2.38 MJ/m^3. Complete data for the other values of maximum strain are reported in Table 1.

3.1.3. Transformation stress and Young's modulus

Fig. 8a illustrates the evolution of the effective Young's modulus, E, as a function of the number of mechanical cycles during material stabilization (cycle # < N_s), while Fig. 8b shows the evolution of the direct transformation stress, σ_s^{AM}. Both parameters exhibit a marked decrease in the first few cycles, and these effects become more evident when increasing the maximum strain ε_{max}. This result can be attributed to the formation of a heterogeneous microstructure, *i.e.* to several microstructural mechanisms occurring during stabilization process, such as the formation of stabilized martensite, detwinning, grain reorientation and slips deformations [38,39]. This heterogeneous microstructure is characterized by an effective Young's modulus which is between those of austenite (E_A) and martensite (E_M), as illustrated in Fig. 8a. In particular, a marked reduction, down to 45 GPa, has been recorded for ε_{max} = 4.5%.

Similar considerations apply to the direct transformation stress, where the formation and accumulation of stabilized martensite, as well as the presence of a heterogeneous structure, cause a decrease of the critical stress to transform austenite to martensite together with a larger range of stress transformation and an increase of the slopes of the stress–strain plateau. In fact, dislocations could play a similar role to strain hardening in plasticity and the increased dislocation density cause the formation of internal stresses that could assist the formation of stress induced martensite [40–43]. In particular, a marked reduction of σ_s^{AM}, from 450 MPa to 215 MPa, has been observed for ε_{max} = 4.5%, while a decrease from 450 MPa to 355 was recorded for ε_{max} = 1.0%. No value is reported for the lowest applied strain, ε_{max} = 0.7%, because it is very close to the elastic response of the material and the onset of stress-induced phase transformation mechanisms cannot clearly identified. Complete data for the other values of maximum strain are reported in Table 1.

3.1.4. Transformation temperatures

Calorimetry tests were carried out on samples subjected to mechanical cycling. The DSC thermograms revealed to be similar to that of *as received* material (see Fig. 1b). In particular, a two-stage transformation is observed during cooling (*B2-R-B19′*), while a one-stage transformation (*B19′-B2*) characterizes the heating branch of the curve. The results, in terms of peak temperatures, are summarized in Fig. 9. Increasing the maximum strain (ε_{max}), the *R-B19′* peak shifts toward lower temperature (from −67 °C to −60 °C), while the effect of ε_{max} on the other two peak temperatures is less pronounced. The irreversible plastic strain induced on the specimens by deformation and by transformation cycling promotes the stabilization of the R-martensite. Indeed, likewise Ti_3Ni_4 precipitates, higher density of dislocations acts as a resistance to lattice distortion due to the transformation from austenite to martensite, and the resistance is much more significant for transformation involving large lattice distortion like *B19′* transformation, while the effect becomes less considerable for transformation involving small lattice distortion like R-transformation [1]. Therefore, the introduction of dislocations by fatigue cycles leads to a decrease of the *R-B19′* characteristic temperatures. It is worth to note that mechanical cycling and formation of lattice defects are also likely responsible for the stabilization of martensite regions [40–43]. Deeper structural investigations are needed for an utter understanding of the microstructural alterations owing to mechanical cycling which lead to a resulting modification of the functional and mechanical properties characteristic of the material.

3.2. Structural fatigue

In the following subsection fatigue data are analyzed by a modified Coffin–Manson approach [37]. Furthermore, scanning electron microscopic observations of the fracture surface are reported and analyzed to better understand the failure mode under different values of the applied strain.

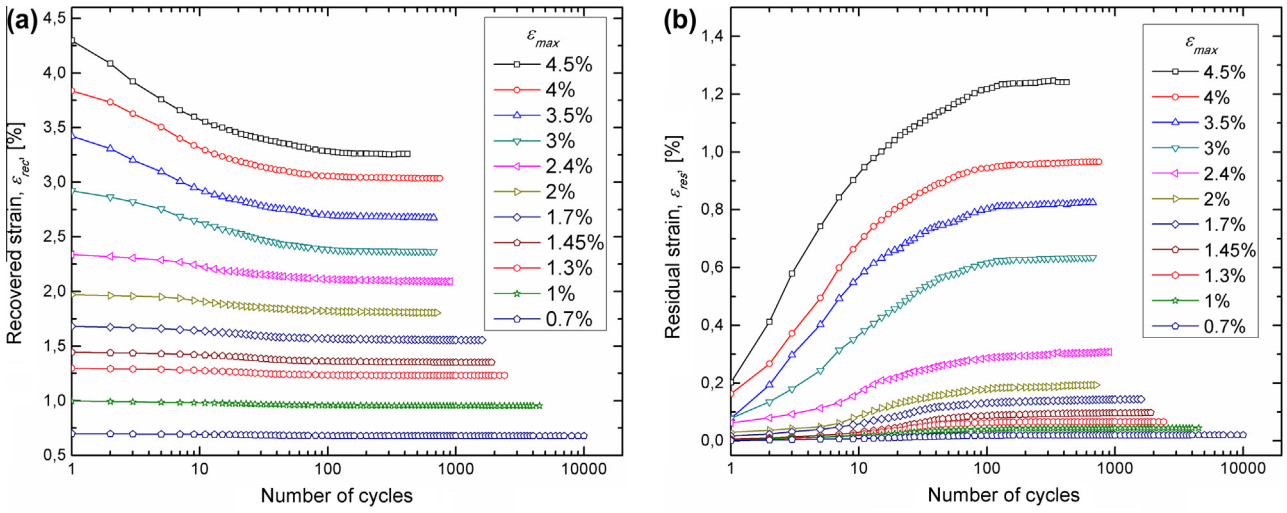

Fig. 4. Evolution of recovery strain ε_{rec} (a) and of the residual strain ε_{res} (b) as a function of the number of mechanical cycles and for different values of the maximum applied strain ε_{max}.

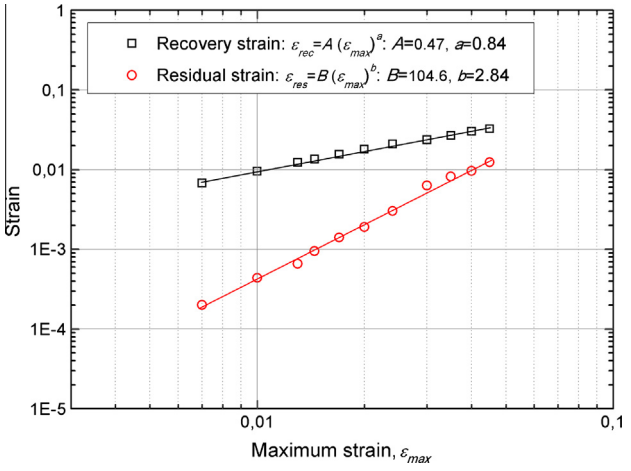

Fig. 5. Stabilized values of the recovery (ε_{rec}) and residual (ε_{res}) strains, as a function of the maximum applied strain ε_{max}.

3.2.1. Modified Coffin–Manson approach

A summary description of the modified Coffin Manson approach, which was proposed by the authors [37], is reported in the following for the sake of completeness. The strain amplitude, $\varepsilon_a = \varepsilon/2$ (see Fig. 2), can be decomposed in the elastic strain amplitude, $\varepsilon_{ae} = \varepsilon_e/2$, and inelastic strain, $\varepsilon_{ai} = \varepsilon_i/2$, which can be regarded as the pseudoelastic recovery:

$$\varepsilon_a = \varepsilon_{ae} + \varepsilon_{ai} \tag{1}$$

where the elastic strain is calculated based on the assumption of linear evolution of the martensite fraction, ξ_M, along the stress–strain transformation plateau and on the use of the Reuss's formula to estimate the Young's modulus, $E(\xi_M)$ (see Refs. [45,46]):

$$\Delta\varepsilon_e = \frac{\sigma}{E(\xi_M)} \tag{2}$$

Fig. 10 illustrates the elastic, inelastic and total strain amplitude (ε_{ae}, ε_{ai} and ε_a) as a function of the number of cycle reversals to failure ($2N_f$) in a log–log diagram.

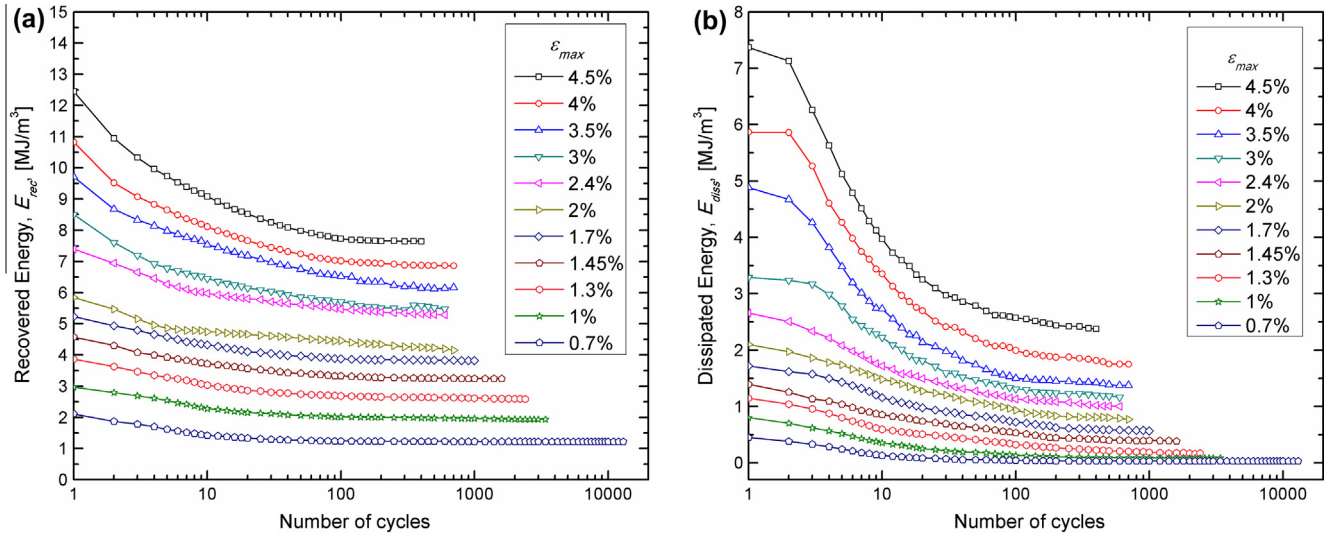

Fig. 6. Evolution of recovery energy E_{rec} (a) and of the dissipated energy E_{diss} (b) as a function of the number of mechanical cycles and for different values of the maximum applied strain ε_{max}.

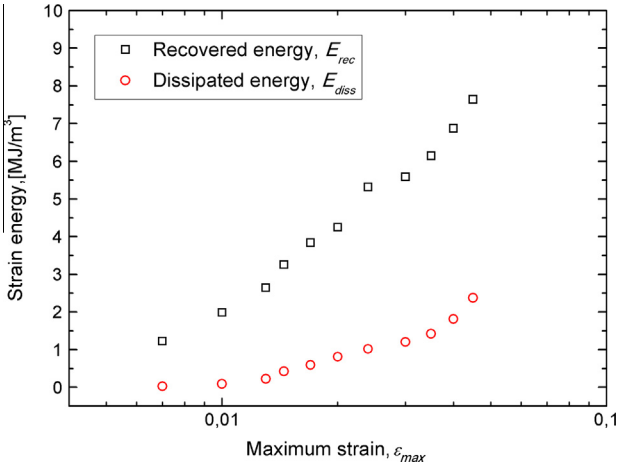

Fig. 7. Stabilized values of the recovery and dissipated energies, E_{rec} and E_{diss}, as a function of the maximum applied strain ε_{max}.

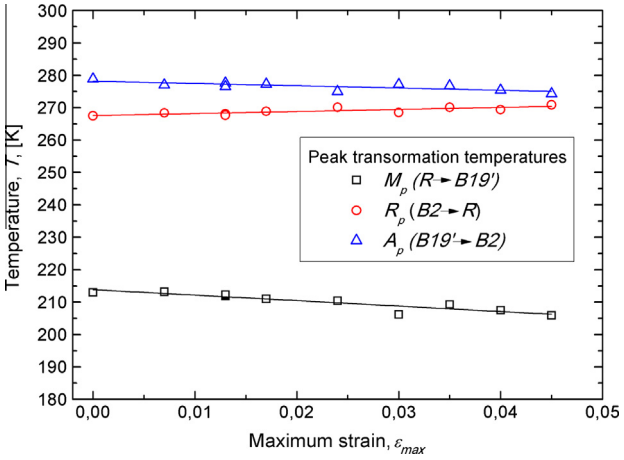

Fig. 9. Evolution of the peak transformation temperatures (R_p, M_p and A_p) versus the maximum applied strain ε_{max}.

Furthermore, the figure shows that both elastic and inelastic strain amplitude (ε_{ae} and ε_{ai}) are well approximated by straight lines in the log–log diagram and, consequently, the two strain components can be expressed by a power law relations in the $\varepsilon_a - 2N_f$ diagram, likewise to Coffin–Manson approach in common engineering metals. In particular, the total strain amplitude, ε_a, can be related to the cycle reversals to failure, $2N_f$, based on a modified Coffin–Manson approach:

$$\varepsilon_a = \varepsilon_{ae} + \varepsilon_{ai} = C(2N_f)^c + D(2N_f)^d \tag{3}$$

where the coefficients C and D and the exponents c and d obtained from the experiments are reported in Fig. 10. It is worth noting that these values have been obtained from a fitting of the experimental data, *i.e.* they are related to specific specimen geometry and loading conditions and, consequently, they should be considered as testing parameters. However, the transferability of the proposed model to the engineering community, *i.e.* to predict fatigue life under generic loading conditions, requires further systematic experimental tests. Furthermore, the results presented in this paper have been obtained with maximum deformation within the stress-induced transformation regime and, consequently, the fatigue response of the material

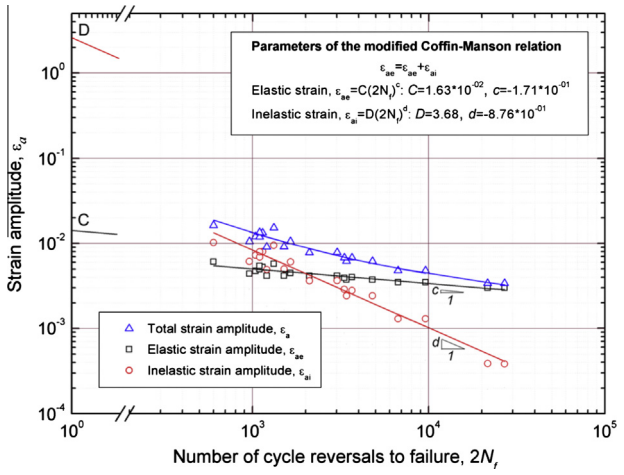

Fig. 10. Fatigue data analysis by the modified Coffin–Manson approach [37].

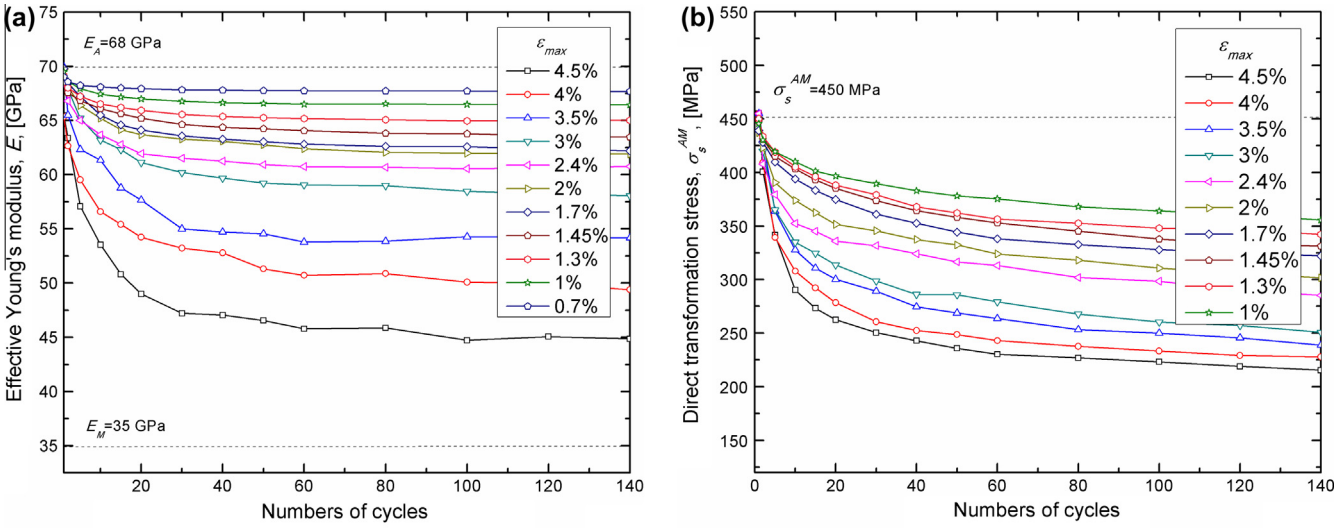

Fig. 8. Evolution of Young's modulus, E, (a) and of the direct transformation stress, σ_s^{AM}, (b) as a function of the number of mechanical cycles and for different values of the maximum applied strain ε_{max}.

in the full austenitic and martensitic regions has not been investigated.

3.2.2. SEM analyses of the fracture surfaces

In Fig. 11, SEM micrographs of the fracture surfaces obtained by testing the samples at different values of maximum deformation (a. 0.7%, b. 1.3%, c. 1.45%, d. 1.7%) are reported.

The analysis revealed that crack initiation occurs at the lateral surface of the specimens, as a consequence of the surface defects produced by the cutting process. In fact, these irregularities lead to local stress concentrations and act as preferable nucleation sites. Furthermore, fracture surfaces show two distinct regions characterized by different morphologies. In particular, the right part of the surfaces in the SEM micrographs of Fig. 11 are characterized by fatigue striations, which are attributed to the stable crack growth resulting from fatigue loads, while the left sides show dimples structures typical of ductile overload fractures. In addition, as expected, the stable crack penetration area decreases with increasing of the maximum applied deformation, ranging from about 2.8 mm at ε_{max} = 0.7% to 0.8 mm at ε_{max} = 1.7%.

4. Conclusion

Strain controlled fatigue tests of a commercial pseudoelastic NiTi alloy were carried out within the stress-induced transformation regime. Both functional and structural fatigue were analyzed,

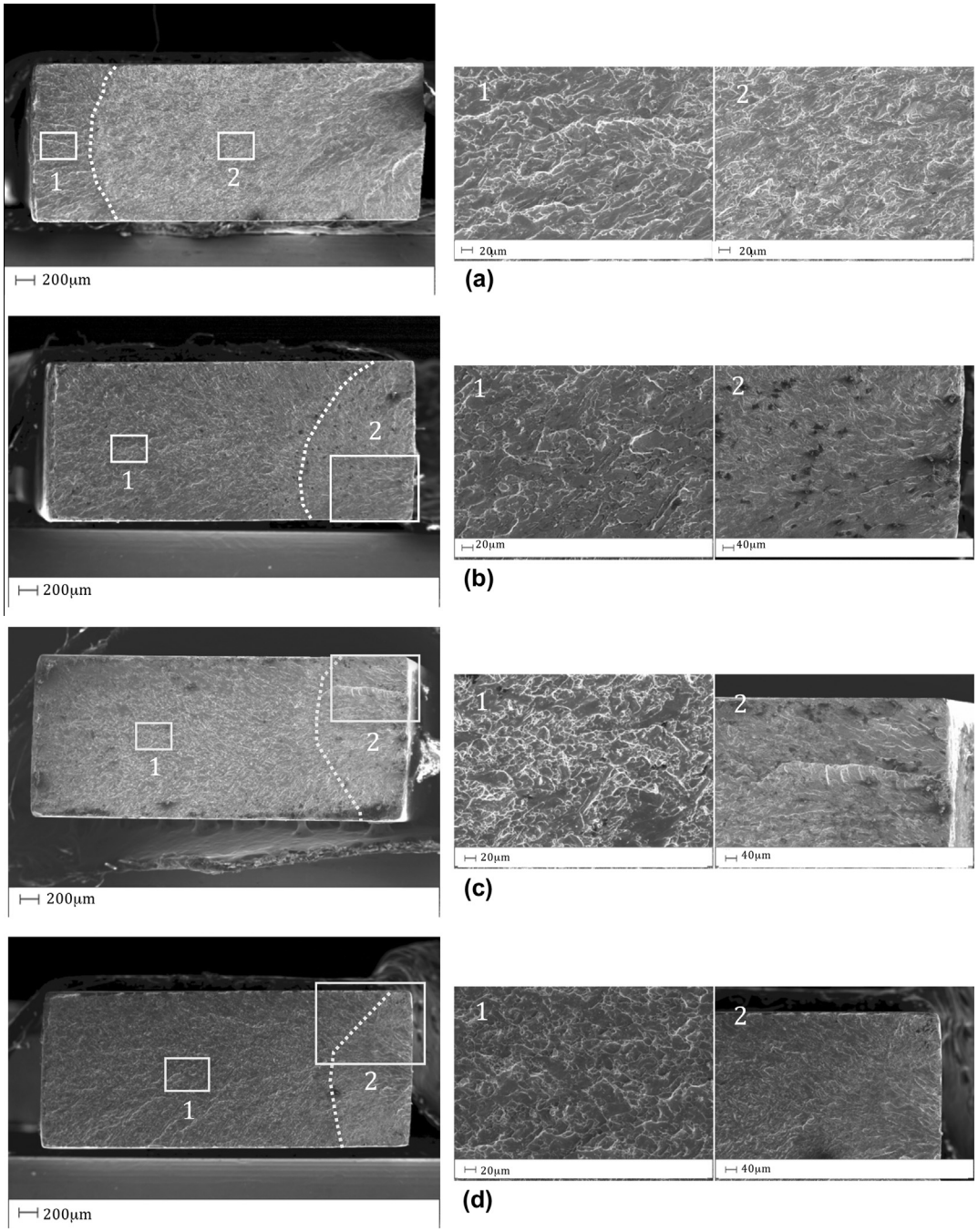

Fig. 11. SEM micrographs of the fracture surfaces with highlight of the stable (right) and unstable (left) crack growth path obtained from specimens tested at different values of maximum deformation: (a) 0.7%, (b) 1.3%, (c) 1.45% and (d) 1.7%.

i.e. the evolution of the pseudoelastic capability and the cycles to failure. The results revealed a degradation of the pseudoelastic recovery, during the first mechanical cycles, and this effect becomes more evident when increasing the strain amplitude. However, a stable functional response is always observed after the first stabilization cycles, which occurs between 100 and 150 cycles. Furthermore, structural fatigue data have been analyzed by a novel strain-life model, based on a modified Coffin–Manson approach. Finally, fracture surfaces have been analyzed by SEM observation in order to study the stable and unstable crack growth mechanisms. However, future experimental tests should be carried out to validate the model and, consequently, to allow a direct transferability of the fatigue data to the engineering community.

Acknowledgment

The authors wish to thank Giordano Carcano (CNR IENi Lecco) for SEM technical assistance.

References

[1] Otsuka K, Ren X. Physical metallurgy of TiNi-based shape memory alloys. Progr Mater Sci 2005;50:511–678.
[2] Melton KN, Mercier O. Fatigue of NiTi thermoelastic martensites. Acta Metall 1979;27:137–44.
[3] Hornbogen E. Review thermo-mechanical fatigue of shape memory alloys. J Mater Sci 2004;39:385–99.
[4] Pelton AR. Nitinol fatigue: a review of microstructures and mechanisms. J Mater Eng Perform 2011;20:613–7.
[5] Miyazaki S, Imai T, Igo Y, Otsuka K. Effect of cyclic deformation on the pseudoelasticty characteristics of Ti–Ni alloys. Metall Trans A 1986;17:115–20.
[6] Tobushi H, Shimeno Y, Hachisuka T, Tanaka K. Influence of strain rate on superelastic properties of TiNi shape memory alloy. Mech Mater 1998;30:141–50.
[7] Lagoudas DC, Miller DA, Rong L, Kumar PK. Thermomchanical fatigue of shape memory alloys. Smart Mater Struct 2009;18. Art no. 085021.
[8] Soul H, Isalgue A, Yamny A, Torra V, Lovey FC. Pseudoelastic fatigue of NiTi wires: frequency and size effects on damping capacity. Smart Mater Struct 2010;19:1–7.
[9] Miyazaki S, Mizukoshi K, Ueki T, Sakuma T, Liu Y. Fatigue life of Ti-50 at.% Ni and Ti–40Ni–10Cu (at.%) shape memory alloy wires. Mater Sci Eng A 2010;273275:658–63.
[10] Tobushi H, Nakahara T, Shimeno Y, Hashimoto T. Low-cycle fatigue of TiNi shape memory alloy and formulation of fatigue life. J Eng Mater – Trans ASME 2000;122:186–91.
[11] Eggeler G, Hornbogen E, Yawny A, Heckmann A, Wagner M. Structural and functional fatigue of NiTi shape memory alloys. Mater Sci Eng A – Struct 2004;378:24–33.
[12] Figueiredo AM, Modenesi P, Buono V. Low-cycle fatigue life of superelastic NiTi wires. Int J Fatigue 2009;31:751–8.
[13] Kollerov M, Lukina E, Gusev D, Mason P, Wagstaff P. Impact of material structure on the fatigue behaviour of NiTi leading to a modified Coffin–Manson equation. Mater Sci Eng A 2013;585:356–62.
[14] Bertacchini OW, Lagoudas DC, Patoor E. Fatigue life characterization of shape memory alloys undergoing thermomechanical cyclic loading. Proc SPIE – Int Soc Opt Eng 2003;5053:612–24.
[15] Rahim M, Frenzel J, Frotscher M, Pfetzing-Micklich J, Steegmuller R, Wohlschlogel M, et al. Impurity levels and fatigue lives of pseudoelastic NiTi shape memory alloys. Acta Mater 2013;61:3667–86.
[16] Scirè Mammano G, Dragoni E. Functional fatigue of Ni–Ti shape memory wires under various loading conditions. Int J Fatigue 2012, in press, Corrected proof.
[17] Nemat-Nasser S, Guo WG. Superelastic and cyclic response of NiTi SMA at various strain rates and temperatures. Mech Mater 2006;38:463474.
[18] Kang G, Kan Q, Yu C, Song D, Liu Y. Whole-life transformation ratchetting and fatigue of super-elastic NiTi Alloy under uniaxial stress-controlled cyclic loading. Mater Sci Eng A Struct 2012;535:228–34.
[19] Casciati S, Marzi A. Fatigue tests on SMA bars in span control. Eng Struct 2011;33:1232–9.
[20] McKelvey AL, Ritchie RO. Fatigue-crack propagation in Nitinol, a shape-memory and superelastic endovascular stent material. J Biomed Mater Res 1999;47:301–8.
[21] McKelvey AL, Ritchie RO. Fatigue-crack growth behavior in the superelastic and shape-memory alloy Nitinol. Metall Mater Trans A 2011;32A:731–43.
[22] Runciman A, Xu D, Pelton AR, Ritchie RO. An equivalent strain/Coffin–Manson approach to multiaxial fatigue and life prediction in superelastic Nitinol medical devices. Biomaterials 2011;32:4987–93.
[23] Moumni Z, Van Herpen A, Riberty P. Fatigue analysis of shape memory alloys: energy approach. Smart Mater Struct 2005;14:287–92.
[24] Gollerthan S, Young ML, Baruj A, Frenzel J, Schmahl WW, Eggeler G. Fracture mechanics and microstructure in NiTi shape memory alloys. Acta Mater 2009;57:1015–25.
[25] Maletta C, Furgiuele F. Analytical modeling of stress induced martensitic transformation in the crack tip region of nickel titanium alloys. Acta Mater 2010;58:92–101.
[26] Maletta C, Young ML. Stress-induced martensite in front of crack tips in NiTi shape memory alloys: modeling versus experiments. J Mat Eng Perform 2011;20(4–5):597–604.
[27] Baxevanis T, Lagoudas D. A mode I fracture analysis of a center-cracked in NiTi shape memory alloy panel under plane stress. Int J Fract 2012;175(2):151–66.
[28] Maletta C, Furgiuele F. Fracture control parameters for NiTi based shape memory alloys. Int J Solids Struct 2011;48(11–12):1658–64.
[29] Maletta C, Sgambitterra E, Furgiuele F. Crack tip stress distribution and stress intensity factor in shape memory alloys. Fatigue Fract Eng Mater 2013;36(9):903–12.
[30] Pelton AR, Schroeder V, Mitchell MR, Gong XY, Barney M, Robertson SW. Fatigue and durability of Nitinol stents. J Mech Behav Biomed 2008;1:153–64.
[31] Gall K, Sehitoglu H, Chumlyakov YI, Kireeva IV. Pseudoelastic cyclic stress–strain response of over-aged single crystal Ti-50.8at% Ni. Scripta Mater 1999;40(1):712.
[32] Sehitoglu H, Anderson R, Karaman I, Gall K, Chumlyakov Y. Cyclic deformation behavior of single crystal NiTi. Mater Sci Eng A – Struct 2001;314:6774.
[33] Dolce M, Cardone D. Mechanical behavior of shape memory alloys for seismic applications austenite NiTi wires subjected to tension. Int J Mech Sci 2001;43:2657–77.
[34] Torra V, Isalgue A, Carreras G, Lovey FC, Soul H, Terriault P, et al. Experimental study of damping in civil engineering structures using smart materials (NiTi – SMA). Application to stayed cables for bridges. Int Rev Mech Eng 2010;4(5):601–11.
[35] Casati R, Tuissi A. Effect of current pulses on fatigue of thin NiTi wires for shape memory actuators. J Mater Eng Perform 2012;21(12):2633–7.
[36] Casati R, Passaretti F, Tuissi A. Effect of electrical heating conditions on functional fatigue of thin NiTi wire for shape memory actuators. Procedia Eng 2011;10:3423–8.
[37] Maletta C, Sgambitterra E, Furgiuele F, Casati R, Tuissi A. Fatigue of pseudoelastic NiTi within the stress-induced transformation regime: a modified Coffin–Manson approach. Smart Mater Struct 2012;21(11):1–9. Art. no. 112001.
[38] Miyazaki S, Imai T, Igo Y, Otsuka K. Effect of cycling deformation on the pseudoelasticity characterisitc of Ni–Ti alloys. Acta Metall 1986;17:115–20.
[39] Miyazaki S. Thermal and stress cycling effects and fatigue properties of Ni–Ti alloys. In: Duerig TW, Melton KN, Stoeckel D, Wayman CM, editors. Engineering aspects of shape memory alloys. London: Butterworth-Heinemann Ltd.; 1990. p. 394–413.
[40] Lin HC, Wu SK, Chou TS, Kao HP. The effects of cold rolling on the martensitic transformation of an equiatomic TiNi alloy. Acta Metall Mater 1991;39(9):2069.
[41] Piao M, Otsuka K, Miyazaki S, Horikawa H. Mechanism of the A_s temperature increase by pre-deformation in thermoelastic alloys. Mater Trans JIM 1993;34(10):919.
[42] Tan G, Liu Y. Comparative study of deformation-induced martensite stabilisation via martensite reorientation and stress-induced martensitic transformation in NiTi. Intermetallics 2004;12(4):373.
[43] Liu Y, Tan G, Miyazaki S. Deformation-induced martensite stabilisation in [100] single-crystalline Ni–Ti. Mater Sci Eng A 2006;438–440:612.
[44] Stephens RI, Fatemi A, Stephens RR, Fuchs HO. Metal fatigue in engineering. 2nd ed. New York: Wiley-Interscience; 2000.
[45] Maletta C, Falvo A, Furgiuele F, Reddy JN. A phenomenological model for superelasticity in NiTi alloys. Smart Mater Struct 2009;18:1–9.
[46] Auricchio F, Sacco E. A one-dimensional model for superelastic shape memory alloys with different elastic properties between austenite and martensite. Int J Non-linear Mech 1997;32:1101–14.